Title: Toward 3D DNA Industrial Nanorobots

Authors:

Feng Zhou[1,2,3]*, Heng Ni[2], Guolong Zhu[2,4], Lev Bershadsky[2], Ruojie Sha[3,]*, Nadrian C. Seeman[3], Paul M. Chaikin[2,]*

Affiliations:

[1]Institute of Biomedical Engineering, Ningbo Cixi Institute of Biomedical Engineering, Ningbo Institute of Materials Technology and Engineering, Chinese Academy of Sciences; Ningbo, China.

[2]Department of Physics, New York University; New York, NY, USA.

[3]Department of Chemistry, New York University; New York, NY, USA.

[4]Department of Chemistry, Biochemistry, and Physics, Fairleigh Dickinson University, Madison, NJ, USA.

*Corresponding author. Email: zhoufeng@nimte.ac.cn (F.Z.); rs17@nyu.edu (R.S.); and Chaikin@nyu.edu (P.M.C.)

Abstract: Nanoscale industrial robots have potential as manufacturing platforms, capable of automatically performing repetitive tasks to handle and produce nanomaterials with consistent precision and accuracy. We demonstrate a DNA industrial nanorobot, that fabricates a 3D optically active, chiral structure from optically inactive parts. By making use of externally controlled temperature and UV light, our programmable robot, ~ 100nm^3 in size, grabs different parts, positions and aligns them so that they can be "welded", releases the construct and returns to its original configuration ready for its next operation. Our robot can also self-replicate its 3D structure and functions, surpassing single-step templating (restricted to 2D) by using folding to access the third dimension and more degrees of freedom. Our introduction of multiple-axis precise folding and positioning as a tool/technology for nano manufacturing will open the door to more complex and useful nano-micro devices.

One-Sentence Summary: We have made DNA industrial nanorobots that can fabricate, manipulate and manufacture nanodevices, and even self-replicate.

Main Text:

INTRODUCTION

Industrial robots, essential to modern manufacturing, take prefabricated parts, align them for further assembly, attach them, deposit them and prepare for their next task. Fabrication of multicomponent systems in both living systems and in industry is done either by self-assembly or by active positioning and fixing/welding the separate parts. Catalysts and enzymes can capture and position two or more components for binding. They are natural industrial robots on the nanoscale(*1, 2*). (By convention industrial robots are automated, programmable and capable of motion on three or more axes(*3, 4*).) Self-assembly is also a powerful technique for equilibrium systems where the thermodynamic or non-equilibrium pathways are preprogrammed into the individual components or the processing techniques(*5-8*), but at present is limited in the complexity of the devices produced.

Artificial nanoscale industrial robots add a new dimension to our nano-micro fabrication toolbox and technologies(*9*).

DNA nanotechnology(*10*) enables the fabrication of many remarkable structures(*11-18*), as well as machines(*17-25*), walkers(*26-30*), enzymes(*31-33*), self-replicators(*34-38*), computers(*39-41*), and even a one shot nano assembly line(*42*). Here as a demonstration, we introduce a simple DNA industrial nanorobot that can manufacture 3D, chiral, left- or right-handed optically active cube corners from optically inactive parts. Our nanorobot is a DNA origami cube corner with three faces $(\sim 100\text{nm})^3$ with DNA sticky end functionalized edges that can be independently programmed for selection, movement and operation on six degrees of freedom. This robot trimer can perform the preprogrammed steps that grab three feedstock DNA origami(*14*) plates out of solution, accurately position them by stepwise folding to close the cube so that the plates edges align and bind by sticky end hybridization. Unlike a single-pot system(42, 43), a user, or external computer program, controls UV light to weld them together by UV crosslinking and changes in temperature releases them into suspension. The plates are decorated with Au nanorods such that the crosslinked cube corner is chiral and optically active unlike the unassembled plates or the robot itself. The industrial robot with its additional folding degrees of freedom also presents a nice solution to the problem of three-dimensional self-replication. Single step Templating in one or two dimensions requires access to the second or third(*37, 38*). Here, with folding for manipulation and positioning, our nondecorated robot cube corner can assemble a complementary cube corner robot and two cycles replicates the original robot. The production then becomes exponential. Our demonstration portends nanomachines and robots programmable and controlled by light and heat for nanoscale production of nanoscale, biocompatible structures and devices.

RESULTS

An outline for the concept, implementation and operation of our DNA industrial robots is found in the Supplementary Text section of the SI. Our 3D fabrication process starts with the construction of the nanorobot, a cube corner shaped DNA origami which is made by self-assembly, folding, and covalent bonding (Fig. 1A). The basic structural unit, effectively a plate, is a cross-tile DNA origami monomer made from perpendicularly organized DNA helices along the two axes(*14*), which allows us to modify the sticky ends on the edges and faces of all four cross extensions (detailed strands information can be found in Fig. S1 and Table S1). Further the cross-tiles exhibit an "=" sign that facilitates AFM identification of their orientation. The robot was made by hybridizing the complementary sticky ends on the origami monomer plates to form a 2D trimer and subsequently folding the semi-flexible-hinged plates 90˚ to fabricate a three-face cube corner using two pairs of strut strands, a short double-stranded DNA, on the adjacent planes. The length of the strut strands was determined to be 45 base pairs, according to the location of the sticky ends on the origami plate, the length of the sticky ends between the origamis and the angle between the two origami plates (Fig. 1C). We further welded the plates to stabilize the 3D structure by the cycloaddition reaction between 4 pairs of photo-cross-linkable 3-cyanovinylcarazole (^{CNV}K)(*43*), a pseudo base, through UV illumination (Fig. 1B). ^{CNV}K and UV for welding formed covalent bonds which were free from detachment throughout the temperature-change process, providing an additional light-controllable degree of freedom. A native gel shows that the folded-welded corner-shaped 3D trimer has a higher mobility than the 2D trimer without folding strut strands, possibly

due to the smaller cross-sectional area of the 3D objects, potentially giving evidence for the formation of the 3D structure in the robot (Fig. 1D). AFM images of the robots present a closed-looped trimer structure with the designed equal sign orientation, confirming the successful crosslinking and formation of the 3D robot (Fig. 1E and S2).

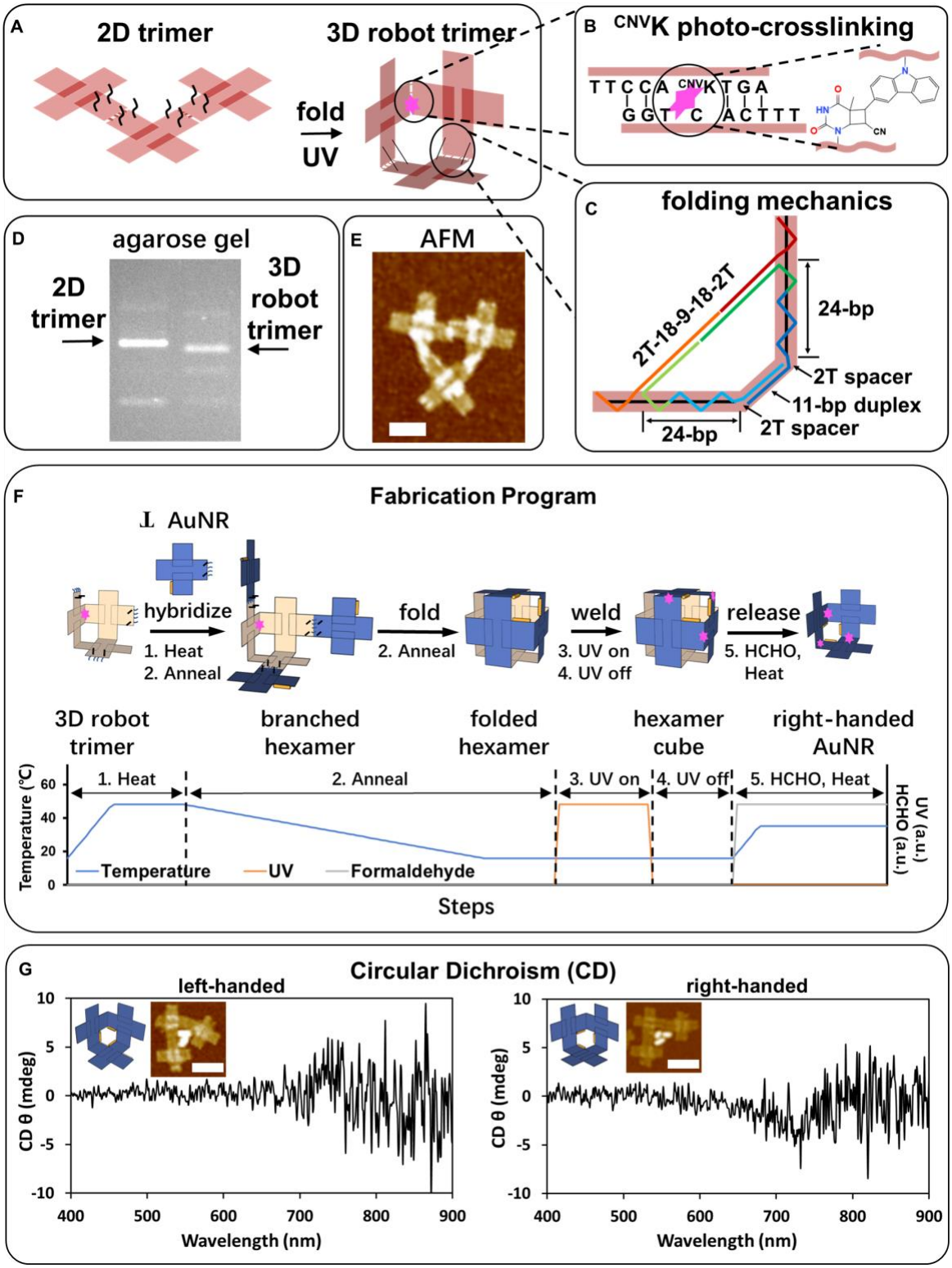

100

Fig. 1. 3D industrial robot - its fabrication, processing flowchart and analysis of its chiral products. Schematics of (A) formation of 3D trimer robots by folding and UV crosslinking (purple star) of 2D trimers *via* (B) photo-crosslinking with ^{CNV}K cycloaddition reaction in the DNA duplex and (C) folding DNA origamis to 90° by two double stranded DNA struts. (D) A non-denaturing agarose gel showing the mobility difference between the 3D robot trimer and 2D trimer. The gel was run at 48 °C. (E) In-air AFM of the 3D seed trimer robot. Note: the DNA trimer robot was stained with uranyl acetate to maintain the structure intact while strongly attracted/flattened to the mica surface(*44*). The robot trimer would break apart without staining (Fig. S3A). (F) Flowchart of the fabrication program for chiral optically active trimer constructs from achiral AuNR monomer plates (top) and pictured preprogramming external control steps and purposes (bottom). Step 1: heat the mixture in incubator at 40 °C for 30 min. Step 2: anneal to 16 °C at a rate of 1 °C/hr. Robot trimer hybridizes epitaxially with three plates to form a branched hexamer. On further cooling, struts similar to those in Fig. 1C precisely fold the plates 90° inward to form a closed cube. Step 3: turn on 365 nm UV LED light. The three plates in the cube are chemically cross-linked via CNVK cycloaddition reaction. Step 4: stop UV illumination after 20 min. Step 5: Mix with formaldehyde to 30% and heat at 30 °C for 30 min to release robot trimers and product AuNR-trimers. Note: ⊥ AuNR ⇒ tiles have gold nanorods attached perpendicular to the equal sign of the cross-tile origami. (G) Circular dichroism spectra showing different chirality obtained by rearranging the Au nanorods decoration on the plates or by using a differently programmed robot.

Our first demonstration, Fig. 1F, the assembly of chiral optically active trimer constructs proceeds by introduction of the robots into a suspension of decorated monomer plates, cross-tile origami that have been decorated with a 25 nm Au nanorod (AuNR) on one cross extension. The temperature is lowered so that the plates should assemble epitaxially on the edges of robot cube corners. Using their strut strands the programmed robot arms are designed to fold the Au nanorod decorated plates 90˚ inward to form a cubic box. The lowest temperature is set such that plates cannot hybridize at their concentration in suspension. However, when they are assembled by the robot and folded to the right position, a closed cubic box, the sticky ends containing 4 ^{CNV}K strands on the plate edges are held in proximity, their local concentration is increased by ~ 10^6(*45*) and they can hybridize. The sample is illuminated with UV light (365 nm) so that the ^{CNV}K strands can be covalently bound. The three plates together can then form a trimer cube corner with the Au nanorods surrounding the vertex in a right-handed manner (Fig. S4D). On heating, the product trimers should be released from the robot (Fig. S4E).

The undecorated 3D robot and its products should be essentially plasmonic achiral but become plasmonic chiroptical after modification with gold nanorods. All of the parts that we use are made of DNA which should be chiral but interactions with red light are sufficiently weak that no circular dichroism could be observed in our apparatus. The decoration with Au nanorods greatly increases the interaction with light(*46, 47*) and the fabricated nanorod decorated cube corners show their clear difference in handedness in their circular dichroism with inverted peaks at 720 and 800 nm (Fig. 1G). The individual plates, even though nanorod decorated, are flat enough so that the mirror plane through the flat plate renders the system achiral (Fig. S5B).

To validate the fabrication process from the original robots to robot-feedstock cubic boxes, and to the finished product trimers, a non-denaturing gel was conducted to study

intermediate structures without AuNR (Fig. 2). We prepared the robot face plates with and without robot-feedstock plate recognition strands, and the feedstock plates with and without folding strut strands. By design of the experiments (details in SI), we could prepare the assembled structure from monomer plates to hexamer cube, folded and not folded. Lanes 7, 8, 9 and 10 (Fig. 2) represent the intermediate structures in the first cycle of fabrication from cube corner robot to robot-feedstock cubic box. After mixing the initial robot trimer with the excess monomer plates (no folding strut strands) and annealing from 48 to 25 ˚C, the all-trimer band moved up to the open-branch hexamer band from lane 7 to lane 8, indicating the self-assembly of three feedstock plates (F) to three edges of the cube corner robot. When the folding strut strands were present, the open-branch hexamer band moved down to the closed-cube hexamer band from lane 8 to lane 9, exhibiting the similar mobility change due to the reduced cross-sectional area like that from the 2D to the 3D trimer (Fig. 1C) and from flat dimer (lane 15) to the folded dimers (lane 2 and 14). The hexamer band barely shifted between lane 9 and lane 10, indicating that the UV-crosslinked hexamer remains the same cubic box. In addition, we compared the open-branched, unfolded nanorobot-feedstock tetramer (Lane 4), pentamer (lane 5) and hexamer (Lane 8), with the folded tetramer (Lane 12), pentamer (lane 11) and hexamer (lane 9). The clear stepwise change in the mobility (Lane 4, 5, and 8) indicates that the shape was changed over the assembly of more feedstock plates on the DNA nanorobots. However, the mobility of the corresponding folded structures (lane 12, 11, 9) showed much smaller difference compared to the unfolded structure (Lane 4, 5, 8), indicating that all three folded structures shared the similar cross-sectional area like the box.

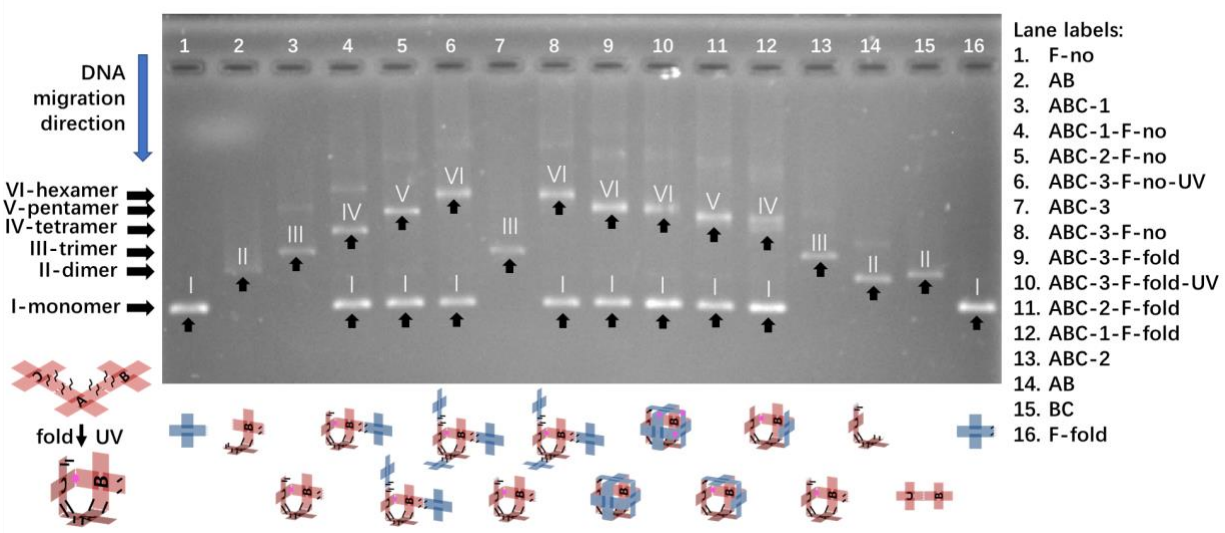

Fig. 2. A non-denaturing gel showing the intermediate structures during the robot fabrication and the steps in the assembly of the designed products. The 0.8% agarose gel was run at 25 ºC at 80 V for 4 hr. We synthesized the DNA origami with different sets of sticky ends to fabricate all the intermediates in the nanorobot fabrication process (design details see Supplementary Text S5). The ratio between ABC trimer robot and monomer feedstock plates is 1:6. The example lane label "10. ABC-3-F-fold-UV" stands for: #10 lane - trimer seed made from A, B, C origami tile (each contains folding strut strands) - 3 sets of sticky ends to assemble 3 feedstock plates - containing folding strut strands - UV crosslinked.

The nanorobot we used here assembles a chiral corner cube. By changing the sticky ends and the protocols for selecting, binding, folding and welding we could have made a number of other structures, *e.g.* a simple two-plate elbow or chair. However, the optically active chiral corner cube has the same form and can be made to have the same functionality as the original robot (except that the edge sticky ends are complementary rather than the same). Therefore, our nanorobot can replicate itself either directly or after an intermediate complementary cycle mimicking DNA replicating via its complement. On repeated cycles of cooling, UV illumination, and heating, the number of offspring should grow exponentially with the number of cycles. 3D templated self-replication (SR) is allowed by the additional degrees of freedom enabled by the precise folding.

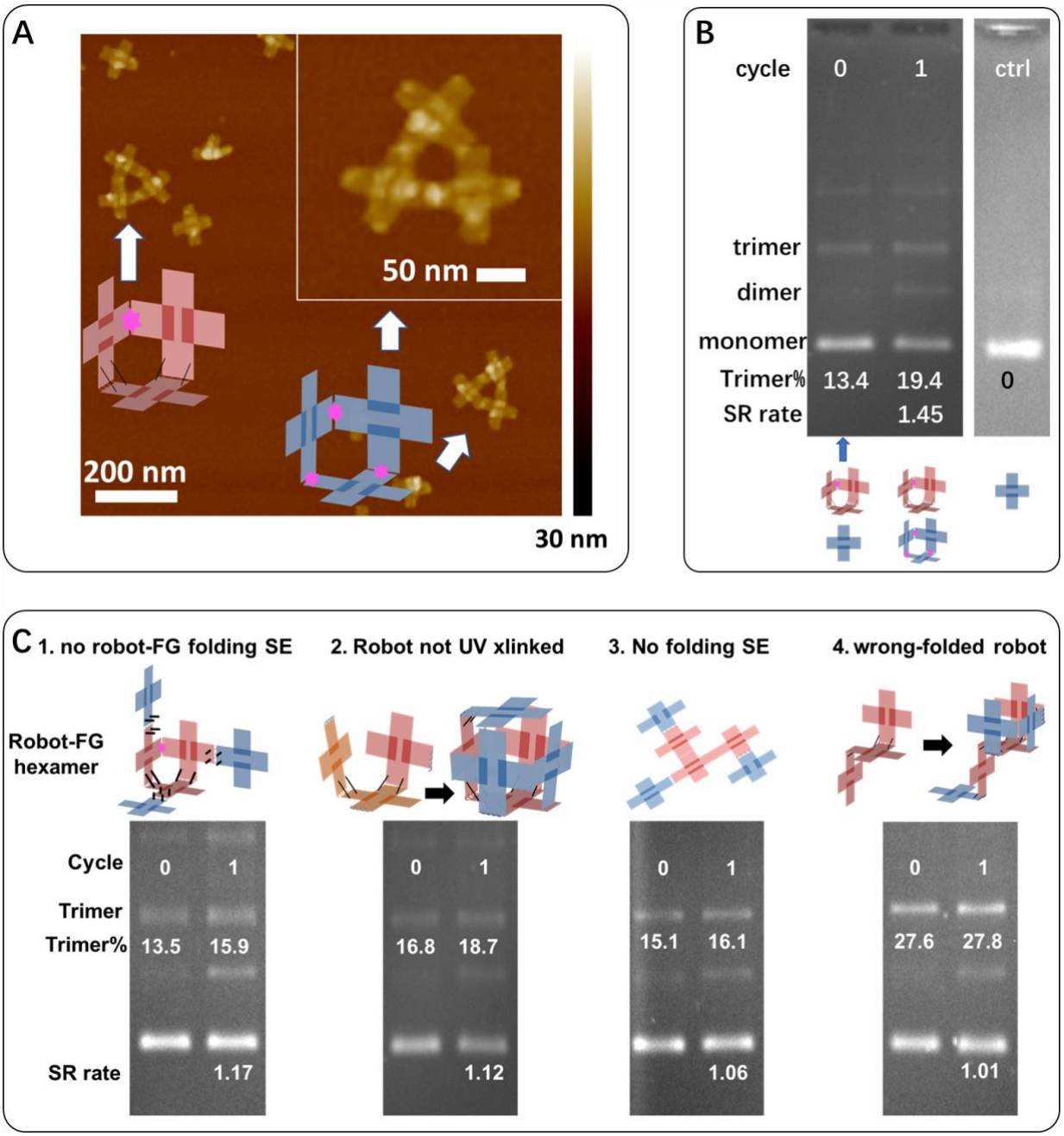

Fig. 3. Analysis of robot-controlled production. (A) After 1 cycle of production, In-air AFM shows the trimer structures with the different orientations of equal sign, enabling us to distinguish between original trimer robots (|| || or = =) and product trimer robots (all ||

=). Note: the DNA trimer was stained with uranyl acetate to show the intact structure while attracted/flattened to the mica surface. (B) A non-denaturing agarose gel shows the self-replication (SR) and quantification of trimer robots after replication, with a starting ratio of 1 : 10 between original robot : monomer plates. Lane ctrl contains the monomer plates after one cycle of the replication process. Any trimers formed without the robot were below the detection limit. (C) Accurate positioning is important. Misfolded robots reduce the assembly efficiency. (1) no folding strands between robot and monomer plate; (2) no UV crosslinking when making 3D robots; (3) no folding strands on robot or monomer plate; and (4) seed robot was folded to the wrong direction. (Top) schematics and (Bottom) corresponding non-denaturing agarose gel images showing the amplification and quantification of trimers after fabrication, with a starting ratio of 1 : 10 between original robot : monomer plate. The robot-assisted fabrication was suppressed with an increase of error to the positioning accuracy.

Figure 3 shows images and gel quantification of the self-replication. The self-replication was conducted by mixing the nanorobot with First Generation, FG, monomer plates at the concentration of 0.15:1.5 nM (Cycle 0). (First generation plates have sticky ends complementary to the robot. Second generation, SG, monomer plates have sticky ends complementary to the FG and the same as the original robot.) After the first cycle of annealing and UV crosslinking (Cycle 1), the same mixture, containing both the robot trimers and the product FG trimers, was run through the non-denaturing gel at 48 ˚C where the FG trimers or monomers were released from the seed robot under heat (Fig. 3B). Due to the same structure between the robot trimer and FG trimer, the gel mobility is the same and there is only one trimer band after self-replication. We use the increase of trimer% from the intensity (I) measurement by gel electrophoresis, 100 * I_trimer / (I_monomer + I_dimer + I_trimer), to quantify the production and self-replication of the robot cube corner trimer (the gel quantification is shown in Fig. S6). The cube corner trimers increased from 13.4% to 19.4%, giving a self-replication rate of 1.45 (replication rate was calculated by trimer% (cyc1) / trimer% (cyc0)), 0.45 offspring per parent (offspring per parent was calculated by trimer% (cyc1) / trimer% (cyc0)-1). Meanwhile, no trimer was detected in the control experiment where only the FG monomer was run at the same annealing-UV illumination condition (Fig. 3B, lane ctrl). The FG trimer is assembled by the robot, not self-assembled on its own. When lowering the UV crosslinking temperature to 4 ˚C, the complementary ^{CNV}K strands on the FG monomers could hybridize and be crosslinked to form flat FG trimer structures without the presence of the robot (Fig. S7). These flat trimers had different mobility than the cube corner trimer. Note that the robot assembly shows an increase of the same trimer band with no observable addition of a flat trimer band. The robot produces its programmed structure, while the non-robot-templated trimer was below the detection limit using gel quantification (Fig. 3B). After release, the structure of both robot and FG trimer product could be found on the AFM image (Fig. 3A and S8), distinguished by the different equal sign orientation, verifying the production process. We identified 58 robot trimers with parallel equal sign and 24 product trimers with perpendicular equal sign (Fig. S8), giving the comparable self-replication rate of 1.41, 0.41 offspring per parent.

For successful fabrication and self-replication, the three face plates of the cube corner need to be placed at the right position so that the complementary ^{CNV}K strands are close enough and at a high local concentration for hybridization. Positioning accuracy is very important for successful UV-crosslinking. For example, in comparison between lane 6 with lane 8 and 10 in Fig. 2, the off-site, unfolded FG plates attached on the robot (lane 8)

were difficult to UV crosslink to form the cubic box (lane 10), and on release to form the FG cube corner. When compared between lane 6 and 8, the hexamer band was unchanged after UV illumination, indicating that the folding is essential in the UV crosslinking of the correct products. To further validate the importance of folding and positioning accuracy, we tried the replication with designed structural errors and evaluated the 1 cycle self-replication rate. We reduced the positioning accuracy from the perfect cube design (Fig. 1F) to the "no plate folding" (Fig. 3C-1), 'Floppy robot (Fig. 3C-2), 'Flat Robot' (Fig. 3C-3) and "wrong-folded robot" (Fig. 3C-4). When the cube corner robot was still intact, the absence of FG-robot folding sticky ends reduces the replication rate by 62.2%, from1.45, 0.45 offspring per parent (Fig. 3B) to 1.17, 0.17 offspring per parent (Fig. 3C-1). Without the folding sticky ends, the FG monomers could fold freely, inward and outward, along the FG-robot hinge which contains 2 thymine single bases in each of the sticky ends (Fig. 1F). Then the local concentration of the complementary ^{CNV}K strands on the assembled FG plates was smaller as was the chance for them to be crosslinked over the UV illumination period, resulting in a smaller replication rate. When the robot was not rigidly crosslinked, the robot center was loose and wobbly, leading to the less successful FG UV crosslinking and a smaller self-replication rate of 1.12, 0.12 offspring per parent (Fig. 3C-2). With more structural errors added to the robot design, we got a much lower self-replication rate, 1.06, 0.06 offspring per parent, on the non-folded flat hexamer structure (Fig. 3C-3), and almost no production using the wrong-folded robot (Fig. 3C-4). Even though there were two FG monomers in the right position on the wrong folded robot, it's still not possible to form the FG trimer structure by UV crosslinking with the free-diffusing FG monomer in the suspension. Thus, the positioning accuracy of all the components of the FG-robot structure are essential in the fabrication of the designed cube-corner product.

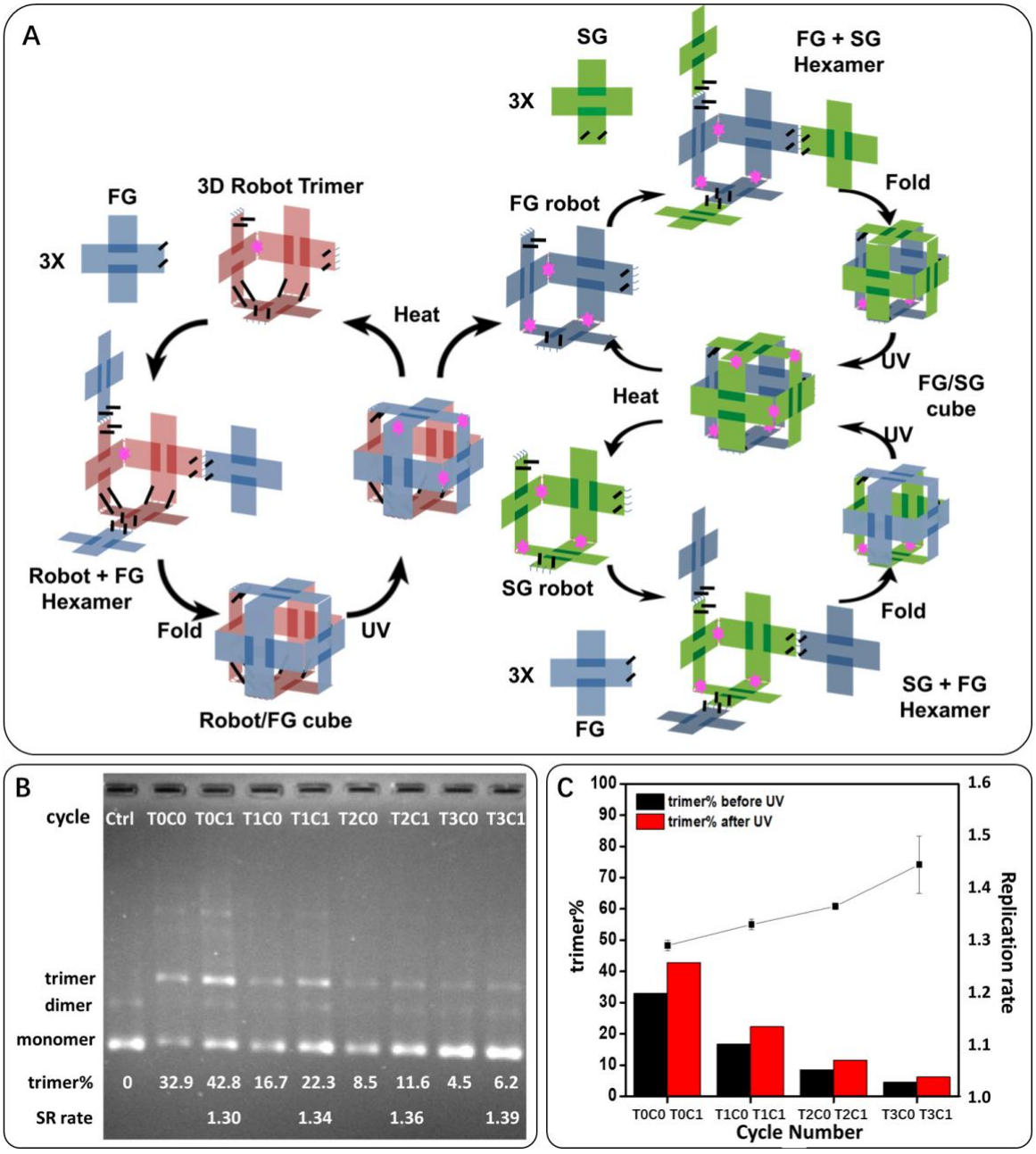

Fig 4. Robot-controlled 3D self-replication. (A) Schematic of self-replication cycles. With the addition of the second-generation (SG) monomer plates, the fabricated FG trimer robots can then act as robot templates to generate further generations. The sticky ends and folding strands are the same on the seed robot (pink) and SG monomer plate (green). The complementary sticky ends and folding strands are on the FG monomer plate (blue). (B) A gel image of four-cycle self-replication of 3D DNA trimer robots using a serial transfer. T_0C_0 in the image represents transfer 0 cycle 0. Explanation of terminology can be found in the materials and methods section. (C) Plot showing the change of the trimer robot percentage and replication rate of each cycle of 3D trimer robot self-replication, obtained from gel data, Figs. 4B and S13A. The gels were run at 48 °C.

After successful one-cycle 3D self-replication, multi-cycle self-replication was conducted by replenishing the UV-illuminated mixture with fresh FG and SG monomers in the subsequent cycles (Fig. 4A). Four cycles of self-replication experiments were conducted

with the starting mixture of initial robots and FG monomer plates at the concentration of 0.5 : 1.5 nM. After UV illumination, 15 µL mixture was replenished with 15 µL 1.5 : 1.5 nM fresh FG : SG stock solutions. After two self-replication cycles, the generation of FG and SG cube corner trimers was confirmed by AFM using equal sign orientations and gold nanoparticle markers (Fig. S9-S12). Both FG and SG trimers had perpendicular equal sign orientations, but FG plates were modified with gold-anchoring sticky ends strands that could attach 5 nm gold nanoparticles after self-replication. The overall trimer percentage was decreased due to the larger monomer dilution factor compared to the trimer self-replication rate (Fig. 4B and S13A). However, the trimer percentage kept increasing for each cycle, with a similar replication rate from 1.3 to 1.39, 0.3 to 0.39 offspring per parent, through four cycles (Fig. 4C and S13 B), indicating the exponential growth of the cube corner trimer structure. A higher replication rate of 1.80 ± 0.01 (N=2), 0.80 offspring per parent, could be obtained when the monomer (FG+SG) to seed robot trimer ratio was higher (3.375 : 0.075 nM), possibly due to the better hexamer assembly (Fig. S19A).

Discussion

For most of the experiments presented in this paper, we have acted as the programming element for our robots, writing down a set of instructions and manually following the predefined program. That consisted of turning on the temperature sweep of the automated incubator and when the temperature reached certain predetermined values, we turned the UV light on or off. At no time did we make any measurements or observations of the sample or make corrections in the preset program. Note that this programmable robot differs from a single pot, bottom-up, molecules-only, system. To avoid any question of human intervention, we setup an electronic device, Adafruit feather cortex M0 microcontroller, which turned on the UV light at a preset temperature and turned it off at a different preset temperature. We then introduced a sample of nanorobots and monomers into the incubator, switched on the incubator and electronic device, waited for the cycle to end, and removed the sample for analysis. The results are shown in Fig. S20 in the SI where the replication yield was 0.47 offspring per parent.

We noted that the degradation in replication rate was higher for these trimer robots (Fig. S19B) than for the dimers we have use more often (ref#37). The production of trimer with robot and FG monomer mirrored this declining rate in the absence of monomer replenishment (Fig. S17B). This phenomenon may well be a consequence of the stronger binding of the daughters to the parents (since there are three bonds on hybridizing rather than the single bonds joining parent trimer to each individual monomer) and hence a more severe consequence of product inhibition. Our hypothesis is that this phenomenon is caused by the cooperative interactions between multiple sets of binding units. While it enables self-assembly at higher temperatures compared to individual sticky ends, it also leads to product inhibition as parent multi-mers have a tendency to bond with daughter multi-mers instead of individual monomers.

In this work, we have discovered an opportunity for process control based on the concentration-dependent nature of product yield or replication growth. We can compensate for the advantage of robot to product binding rather than robot to monomer binding by adding more monomers depending on the product inhibition and its enhancement to cooperative binding.

Conclusion

Our simple nanorobot is a step towards a manufacturing/assembly robot, and can be readily extended to more complex tasks by adding more arms, folding struts, and welders. Here we used only temperature as an actuator and ^{CNV}K and UV for welding. DNA hybridization/dehybridization can be controlled optically with different wavelengths by incorporation of photoisomers, *e.g.*, azobenzenes(*48*), and there are several ways of photo-crosslinking, *e.g*. cinnamate(*49*), psoralen(*50*). Therefore, 3D DNA industrial nanorobots can be made with many controllable degrees of freedom. Since there are many polymers, plastics, metals, and other materials that can be functionalized with DNA, more diverse robots and their products can be fabricated with different compositions. DNA structures and devices are biocompatible and similar in size to organelles. These industrial nanorobots may find biomedical applications as artificial enzymes or organelles.

MATERIALS AND METHODS

Gold, DNA, and purification

5 nm gold nanoparticle in CTAB was purchased from Ted Pella, Inc. 20 nm (20*5*5) and 25 nm (25*5*5 nm) gold nanorods in SDS was purchased from Nanopartz, Inc. Long single stranded scaffold DNA m13mp18 was purchased from Bayou Biolabs. UV crosslinkable ^{CNV}K phosphoramidite was purchased from Glen Research. The single stranded DNA sticky ends containing ^{CNV}K were synthesized on an Applied Biosystems 394 DNA synthesizer. The remaining DNA strands were purchased from Integrated DNA Technology, Inc. The sticky-end strands were purified using denaturing PAGE. The staples strands with thiol group were purified by IDT using HPLC.

Formation of DNA origami tile monomer

Scaffold strands m13mp18 were mixed with the staple strands at the molar ratio of 1 : 8 in the 1X TAE/Mg^{2+} buffer (40 mM Tris · HCl, 20 mM acetic acid, 2.5 mM EDTA, 12.5 mM magnesium acetate, pH 8.0). The final concentration of the scaffold strands was 10 nM. The mixture was placed in a thermocycling incubator through the following ramping procedure:

1. Heat to 70 ˚C at a rate of 99 ˚C/h and stay for 20 min
2. Cool to 20 ˚C at a rate of 7 ˚C/h
3. If running overnight, cool to 4 ˚C at a rate of 99 ˚C/h

The products were purified in 100 MW Millipore Amicon Ultra 0.5-ml centrifugal filter using 1X TAE/Mg^{2+} buffer (10 mM magnesium acetate) for 5 times for the buffer exchange and the removal of excess staple strands.

Gold nanostructure functionalization and attachment on DNA origami

To coat the gold nanoparticles (AuNP) and gold nanorods (AuNR) with DNA, the AuNP and AuNR were centrifuged, and the supernatant was discarded to remove the ligands in the solution. The AuNP and AuNR were stabilized by buffer exchange with the fresh 2.5 mM BSPP solution for five times. 32 μL thiolated DNA (50 μL) and 500 mM TCEP (3 μL) were mixed well and incubated for 1 hour. The mixture was filtered using G25 column at 1K rcf for 1 min to remove TCEP. The AuNP and AuNR solutions were mixed with the reduced thiolated DNA at the ratio of 1:100 for AuNP and 1: 500 for AuNR in 0.5X TBE buffer. The mixture was shaken at r.t. for 1 day. 5 M NaCl solution was added into the mixture to increase the NaCl concentration by 25 mM at each step and the mixture was shaken at r.t. in between. Repeat this step for several times until the final concentration of NaCl was 0.2 M. The mixture was shaken overnight at 30 ˚C and washed by 1X TAE buffer using 100K MW filters at 6000 rpm for 5 time to remove the excess thiolated DNA. The DNA coated AuNP and AuNR was stored in 1X TAE buffer at 4 ˚C.

AuNP and AuNR were mixed with the DNA origami with the complementary gold attachment sticky ends (see Fig. S1) at the ratio of 1:5. The mixture was annealed from 48 ˚C (AuNP) or 40 ˚C (AuNR) to r.t. at the rate of 0.7 ˚C/h. AFM images (Fig. S4A and S4B showed the formation of origami-AuNR monomer is above 95%. The excess AuNR were removed by running 0.8% non-denaturing gel at 40 ˚C. The DNA-AuNR were recovered by gel cutting and electrophoresis elution (80V, 40 ˚C, 0.5 hour forward and 3 min reverse electrophoresis in 3500 MW dialysis bag).

Formation of DNA nanorobot, the seed robot trimer

As shown in Fig. 1A, robot-A, robot-B, and robot-C monomers were preheated to 53 ˚C for 30 min and then mixed at the concentration of 3 : 3 : 3 nM. The mixture was cooled to 16 ˚C at a rate of 0.7 ˚C/h. After confirming the formation of the trimer structure with AFM and gel electrophoresis, the seed robot trimer was diluted to 0.4 nM and UV crosslinked using the 365 nm UV LED light (M365LP1^{c}, Thorlabs Inc, Power intensity is 24 mW/mm^2) at 16 ˚C for 20 min. If prepared at high concentration, hexamer product from inter-trimer hybridization or crosslinking could happen (Fig. S15).

The plasmonic chiroptical robot trimer was made by self-assembly and UV crosslinking of 20 nm AuNR modified robot monomers (Fig. S4C and S5C). The robot trimer with one AuNP marker was made by self-assembly and UV crosslinking AuNP-modified robot monomer A and non-AuNP-modified robot monomer B and C.

Production and self-replication cycling (please see “General remarks on the working of the industrial nanorobot” in Supplementary Text from which this is taken)

The Standard Production and Self-replication was conducted as below:

1. Heating at 48 ˚C for 30 min to break the robot-FG, FG-SG, and strut sticky ends binding.
2. Slow annealing to 16 ˚C at a rate of 1 ˚C/h.
3. UV crosslinking with a 365 UV LED light for 20 min. The environmental temperature was set at 16 ˚C after screening for the lowest temperature without generating non-robot-seeded trimer (Fig. S14A and S14B).

Seven types of production and self-replication were conducted using the DNA nanorobots.

1. Production of AuNR trimers from the undecorated DNA nanorobot (Fig. 1F and 1G):

a) DNA nanorobot was mixed with the gold nanorod modified FG monomer (FG-AuNR) at a ratio of 0.4 : 2 nM; The control without robot trimer has 2 nM FG-AuNR.

b) Reduce the initial heating temperature from 48 to 40 ˚C to prevent the AuNR detachment.

2. One-cycle self-replication using the DNA nanorobot and FG monomer (Fig. 3A, 3B, and S8):

a) DNA nanorobot was mixed with the FG monomer at a ratio of 0.15 : 1.5 nM

b) Standard 3D self-replication procedure.

3. Non-robot-templated control experiment using the FG-AuNP and SG-non-AuNP monomer (Fig. S14C):

a) FG and SG monomer were mixed at a ratio of 1.8 : 1.8 nM

b) Standard 3D self-replication procedure.

4. Multi-cycle self-replication using a serial transfer of fresh FG and SG monomers (Fig. 4B and 4C):

a) 40 μL solution containing 0.5 nM DNA nanorobots and 1.5 nM FG monomers were prepared. 10 μL sample was taken out to quantify the initial trimer nanorobot amount and the rest solution was covered by 50 μL silicone oil (HR3-415, HAMPTON RESEARCH) to prevent the evaporation-induced concentration change. After each cycle of standard 3D self-replication, 10 μL sample was extracted for AFM imaging and non-denaturing gel electrophoresis. An additional 20 μL of fresh 1.5 nM FG and 1.5 nM SG stock solution was transferred into the original tube before the next cycle of 3D self-replication.

b) In Fig. 4B, T_0C_0 in the image represents transfer 0 cycle 0, the sample of seed robot trimer and monomer after mixing. T_0C_1 represents transfer 0 cycle 1, the same sample after 1 cycle replication. T_1C_0 represents transfer 1 cycle 0, the sample after transfer and replenishment with fresh monomers. T_1C_1 represents transfer 1 cycle 1, the sample after transfer and another cycle of self-replication.

5. Two-cycle self-replication with step-wise addition of FG-1AuNP and SG-0AuNP monomer plates (Fig. S9-S12)

a) As shown in Fig. S10, Seed-robot-trimer-1Au was mixed with FG-monomer-1Au at the concentration of 0.15 : 1.5 nM to produce FG-trimer-3Au through the 1st standard self-replication cycle. Then, 8 uL mixture was added to 16 uL solution of 1.5 nM SG-no Au plates and went through the 2nd standard self-replication cycle.

6. Multi-cycle experiments of trimer production with seed robot trimer and FG monomer only (Fig. S17, S18 and S1)

a) Seed robot trimer and FG monomer were mixed at the ratio of 0.2 : 5 nM.

b) Run 4 cycles of standard 3D self-replication procedure. (Fig. S17).

c) After 3 cycle standard procedure, 30 μL T0C3 sample was mixed with 60 μL 5 nM FG feedstock solution to make T1C0. Then, 4 cycles of standard 3D self-replication procedure. (Fig. S18).

7. Multi-cycle self-replication experiments without replenishment (Fig. S19)

a) DNA nanorobot was mixed with the FG and SG monomer at a ratio of 0.075 : 1.8 : 1.575 nM.

b) Run 4 cycles of standard 3D self-replication procedure.

8. No-human-intervention robot-templated production procedure (Fig. S20)

a) DNA nanorobot was mixed with the FG and SG monomer at a ratio of 0.15 : 3.6 : 3.15 nM.

b) Run 1 cycles of standard 3D self-replication procedure using Adafruit feather cortex M0 microcontroller to control the UV light switch.

Non-denaturing Agarose Gel Electrophoresis

0.8% agarose gel was prepared and immersed in the 1X TAE/Mg^{2+} buffer inside the gel electrophoresis box. 5 μL samples were mixed with 1 μL non-denaturing tracking dye (1X TAE/Mg^{2+} buffer, 50% glycerol and trace amount of bromophenol Blue and Xylene Cyanol FF). Gel was run at 4-5 V/cm at 48 ˚C for 3 hours. The gel was immersed in the Ethidium Bromide (EB) solution for staining and rinsed with water to remove excess stain. The fluorescent gel image was processed using ImageJ to quantify the amount of the trimers, dimers, and monomers to calculate the trimer percentage (trimer%). The growth or replication rate of each self-replication cycle was calculated by dividing the trimer% after UV crosslinking over the trimer% before UV crosslinking (Fig. 4B and S13A). When there is no monomer replenishment (Fig. 3B, 3C, S6 and S19), the trimer% before and after UV would be marked as cycle 0 and cycle 1, and the self-replication rate was calculated as trimer% (cyc1) / trimer% (cyc0).

Gel electrophoresis purification was conducted after running the non-denaturing gel. We ran multiple lanes of the sample mixture. We cut out one lane and placed that in the Ethidium Bromide solution for staining. After rinsing and UV illumination to visualize the band position, we cut out the gel containing the target band and placed them in the dialysis bag (MW=3500). A second gel electrophoresis was conducted under the previous condition for 0.5 hr. The eluted solution was collected and concentrated using 100 MW Millipore Amicon Ultra 0.5-ml centrifugal filter at the speed of 300 rcf for 1 hour. The recovering yield was 27% for the AuNR monomer plates, and 14% for the robot trimer (Fig. S16).

AFM imaging

AFM imaging was performed on the Nansocope V Multimode 8 scanning probe microscope (PeakForce QNM Software, ScanAsyst-HR accessory). Silicon nitride tips (ScanAsyst-Air; Bruker Nano, Inc.) were used for peakforce mode in air. Silicon nitride tips (ScanAsyst-liquid; Bruker Nano, Inc.) were used for peakforce mode in liquid.

1. For seed robot trimer formation (Fig. 1E and S2), 2 μL diluted sample was mixed with 4 μL 1% uranyl acetate in 1X TAE/Mg^{2+} solution for 1 min and deposited on a clean mica surface (Ted Pella, Inc.) for 1 min. The mica was then washed with 50–70 μL of ddH_2O three times, and subsequently dried using N_2.
2. For self-replication results (Fig. 3A), the DNA trimer was stained with uranyl acetate to show the intact structure while sitting on the mica surface. The fresh-cleaved mica substrate, 2 μL diluted sample and 4 μL 1% uranyl acetate in 1X TAE/Mg^{2+} solution were heated at 48 ˚C for 30 min. Then following the same mixing, deposition and washing step as demonstrated above to prepare AFM in air sample.
3. For self-replication results marked by AuNR (Fig. 1G, S4, and S5C) or AuNP (Fig. S9-S12, and S14C), the heat-release at 48 ˚C could detach the DNA sticky ends on the gold surface and remove the gold marker from the DNA origami. To lower the dehybridization temperature for heat-release, the samples were mixed with formaldehyde to 30% and the AFM samples were prepared at 30 ˚C.

Circular dichroism

Circular dichroism was conducted on Jasco J-1500 Circular Dichroism Spectrometer with the standard UV-Vis detector. 100 μL sample was placed in the cuvette with the window width of 2 mm and depth of 10 mm. The sample spectra were corrected by the subtraction with the blank measurement of 1X TAE/Mg^{2+} buffer.

Statistical methods

We used the gel results to quantify the growth and compare the self-replication rate and regard the wide-scan AFM data (Fig. S8, S11, S12, and S14C) as semiquantitative corroboration. The statistical data (Fig 4C) were calculated based on gel electrophoresis results in Fig. 4B and S13A. The detailed calculation was included as Fig. S13B.

Supplementary Materials

Supplementary Texts S1 to S14
Figs. S1 to S20 for multiple supplementary figures
Table S1 for the supplementary table
References (37), (44), (45), (51) and (52) for the references only cited in the SM

References and Notes

1. K. Chen, F. H. Arnold, Engineering new catalytic activities in enzymes. *Nat. Catal.* **3**, 203-213 (2020).
2. J. A. Doudna, V. L. Rath, Structure and Function of the Eukaryotic Ribosome: The Next Frontier. *Cell* **109**, 153-156 (2002).
3. V. Zykov, E. Mytilinaios, B. Adams, H. Lipson, Self-reproducing machines. *Nature* **435**, 163-164 (2005).
4. A. Abdel-Rahman, C. Cameron, B. Jenett, M. Smith, N. Gershenfeld, Self-replicating hierarchical modular robotic swarms. *Comms. Eng.* **1**, 35 (2022).
5. S. Li *et al.*, Particle robotics based on statistical mechanics of loosely coupled components. *Nature* **567**, 361-365 (2019).
6. C. A. Mirkin, R. L. Letsinger, R. C. Mucic, J. J. Storhoff, A DNA-based method for rationally assembling nanoparticles into macroscopic materials. *Nature* **382**, 607-609 (1996).
7. W. Liu, J. Halverson, Y. Tian, A. V. Tkachenko, O. Gang, Self-organized architectures from assorted DNA-framed nanoparticles. *Nat. Chem.* **8**, 867-873 (2016).
8. A. Kuzyk *et al.*, DNA-based self-assembly of chiral plasmonic nanostructures with tailored optical response. *Nature* **483**, 311-314 (2012).
9. S. Kassem, A. T. Lee, D. A. Leigh, A. Markevicius, J. Solà, Pick-up, transport and release of a molecular cargo using a small-molecule robotic arm. *Nat. Chem.* **8**, 138-143 (2016).
10. N. C. Seeman, *Structural DNA nanotechnology*. (Cambridge University Press, 2015).
11. P. W. Rothemund, Folding DNA to create nanoscale shapes and patterns. *Nature* **440**, 297-302 (2006).
12. S. M. Douglas *et al.*, Self-assembly of DNA into nanoscale three-dimensional shapes. *Nature* **459**, 414-418 (2009).
13. E. S. Andersen *et al.*, Self-assembly of a nanoscale DNA box with a controllable lid. *Nature* **459**, 73-76 (2009).
14. W. Liu, H. Zhong, R. Wang, N. C. Seeman, Crystalline two-dimensional DNA-origami arrays. *Angew. Chem. Int. Ed.* **50**, 264-267 (2011).

15. N. C. Seeman, H. F. Sleiman, DNA nanotechnology. *Nat. Rev. Mater.* **3**, 1-23 (2017).
16. Y. Ke, T. Meyer, W. M. Shih, G. Bellot, Regulation at a distance of biomolecular interactions using a DNA origami nanoactuator. *Nat. Commun.* **7**, 1-8 (2016).
17. T. Gerling, K. F. Wagenbauer, A. M. Neuner, H. Dietz, Dynamic DNA devices and assemblies formed by shape-complementary, non–base pairing 3D components. *Science* **347**, 1446-1452 (2015).
18. A. E. Marras, L. Zhou, H.-J. Su, C. E. Castro, Programmable motion of DNA origami mechanisms. *Proc. Natl. Acad. Sci. U.S.A.* **112**, 713-718 (2015).
19. G. Zhu *et al.*, Microchemomechanical devices using DNA hybridization. *Proc. Natl. Acad. Sci. U.S.A.* **118**, e2023508118 (2021).
20. B. Yurke, A. J. Turberfield, A. P. Mills, F. C. Simmel, J. L. Neumann, A DNA-fuelled molecular machine made of DNA. *Nature* **406**, 605-608 (2000).
21. R. A. Muscat, J. Bath, A. J. Turberfield, A programmable molecular robot. *Nano Lett.* **11**, 982-987 (2011).
22. E. Kopperger *et al.*, A self-assembled nanoscale robotic arm controlled by electric fields. *Science* **359**, 296-301 (2018).
23. S. M. Douglas, I. Bachelet, G. M. Church, A logic-gated nanorobot for targeted transport of molecular payloads. *Science* **335**, 831-834 (2012).
24. M. Akter *et al.*, Cooperative cargo transportation by a swarm of molecular machines. *Science Robotics* **7**, eabm0677 (2022).
25. L. Liu *et al.*, A localized DNA finite-state machine with temporal resolution. *Science Advances* **8**, eabm9530 (2022).
26. C. Jung, P. Allen, A. Ellington, A stochastic DNA walker that traverses a microparticle surface. *Nat. Nanotechnol.* **11**, 157-163 (2016).
27. W. B. Sherman, N. C. Seeman, A precisely controlled DNA biped walking device. *Nano Lett.* **4**, 1203-1207 (2004).
28. A. J. Thubagere *et al.*, A cargo-sorting DNA robot. *Science* **357**, eaan6558 (2017).
29. X. Qu *et al.*, An exonuclease III-powered, on-particle stochastic DNA walker. *Angew. Chem. Int. Ed.* **56**, 1855-1858 (2017).
30. T. Omabegho, R. Sha, N. C. Seeman, A bipedal DNA Brownian motor with coordinated legs. *Science* **324**, 67-71 (2009).
31. G. Grossi, M. D. E. Jepsen, J. Kjems, E. S. Andersen, Control of enzyme reactions by a reconfigurable DNA nanovault. *Nat. Commun.* **8**, 1-8 (2017).
32. M. Liu *et al.*, A DNA tweezer-actuated enzyme nanoreactor. *Nat. Commun.* **4**, 1-5 (2013).
33. S. Zhao *et al.*, Efficient Intracellular Delivery of RNase A Using DNA Origami Carriers. *ACS Appl. Mater. Interfaces* **11**, 11112 (2019).
34. T. Wang *et al.*, Self-replication of information-bearing nanoscale patterns. *Nature* **478**, 225-228 (2011).
35. R. Schulman, B. Yurke, E. Winfree, Robust self-replication of combinatorial information via crystal growth and scission. *Proc. Natl. Acad. Sci. U.S.A.* **109**, 6405-6410 (2012).
36. T. Li, K. Nicolaou, Chemical self-replication of palindromic duplex DNA. *Nature* **369**, 218-221 (1994).
37. X. He *et al.*, Exponential growth and selection in self-replicating materials from DNA origami rafts. *Nat. Mater.* **16**, 993-997 (2017).
38. R. Zhuo *et al.*, Litters of self-replicating origami cross-tiles. *Proc. Natl. Acad. Sci. U.S.A.* **116**, 1952-1957 (2019).
39. D. Woods *et al.*, Diverse and robust molecular algorithms using reprogrammable DNA self-assembly. *Nature* **567**, 366-372 (2019).
40. X. Xiong *et al.*, Molecular convolutional neural networks with DNA regulatory circuits. *Nat. Mach. Intell.* **4**, 625-635 (2022).

41. G. Chatterjee, N. Dalchau, R. A. Muscat, A. Phillips, G. Seelig, A spatially localized architecture for fast and modular DNA computing. *Nat. Nanotechnol.* **12**, 920-927 (2017).
42. H. Gu, J. Chao, S.-J. Xiao, N. C. Seeman, A proximity-based programmable DNA nanoscale assembly line. *Nature* **465**, 202-205 (2010).
43. Y. Yoshimura, K. Fujimoto, Ultrafast Reversible Photo-Cross-Linking Reaction: Toward in Situ DNA Manipulation. *Org. Lett.* **10**, 3227-3230 (2008).
44. F. Zhou *et al.*, 3D Freestanding DNA Nanostructure Hybrid as a Low-Density High-Strength Material. *ACS nano* **14**, 6582-6588 (2020).
45. F. Zhou, R. Sha, H. Ni, N. Seeman, P. Chaikin, Mutations in artificial self-replicating tiles: A step toward Darwinian evolution. *Proc. Natl. Acad. Sci. U.S.A.* **118**, e2111193118 (2021).
46. A. Kuzyk *et al.*, Reconfigurable 3D plasmonic metamolecules. *Nat. Mater.* **13**, 862-866 (2014).
47. L. Xin, X. Duan, N. Liu, Dimerization and oligomerization of DNA-assembled building blocks for controlled multi-motion in high-order architectures. *Nat. Commun.* **12**, 3207 (2021).
48. H. Asanuma *et al.*, Synthesis of azobenzene-tethered DNA for reversible photo-regulation of DNA functions: hybridization and transcription. *Nat. Protoc.* **2**, 203-212 (2007).
49. L. Feng *et al.*, Cinnamate-based DNA photolithography. *Nat. Mater.* **12**, 747-753 (2013).
50. S. T. Isaacs, C.-K. J. Shen, J. E. Hearst, H. Rapoport, Synthesis and characterization of new psoralen derivatives with superior photoreactivity with DNA and RNA. *Biochemistry* **16**, 1058-1064 (1977).
51. J. B. Mills, E. Vacano, P. J. Hagerman, Flexibility of single-stranded DNA: use of gapped duplex helices to determine the persistence lengths of Poly(dT) and Poly(dA). *J. Mol. Biol.* **285**, 245-257 (1999).
52. H. Ni *et al.*, Direct visualization of floppy two-dimensional DNA origami using cryogenic electron microscopy. *iScience* **25**, 104373 (2022).

Acknowledgments:

Funding:

Department of Energy DE-SC0007991 (PMC, NCS, RS, FZ)

Department of Energy DE-SC0020976 (PMC)

Center for Bio-Inspired Energy Sciences, an Energy Frontier Research Center funded by the Department of Energy, Office of Sciences, Basic Energy Sciences, DE-SC0000989 (PMC, HN, GZ, LB)

National Science Foundation 2106790 (RS, NCS)

Office of Naval Research N000141912596 (RS, NCS)
Human Frontiers Science Program RGP0010/2017 (RS, NCS)

Author contributions:

Conceptualization: PMC, NCS, RS, FZ
Methodology: RS, FZ, HN, GZ, LB
Investigation: PMC, NCS, RS, FZ, HN, GZ, LB
Visualization: FZ, HN, GZ, LB
Funding acquisition: PMC, NCS
Project administration: PMC, NCS
Supervision: PMC, NCS

Writing – original draft: PMC, NCS, FZ
Writing – review & editing: PMC, NCS, RS, FZ, HN, GZ, LB

Competing interests: Authors declare that they have no competing interests.

Data and materials availability: All data are available in the main text or the supplementary materials.